2018 European Control Conference (ECC)
June 12-15, 2018. Limassol, Cyprus

Predictive Torque Vectoring Control with Active Trail-Braking

Konstantinos Zarkadis, Efstathios Velenis, Efstathios Siampis and Stefano Longo

Abstract— **In this work we present the development of a torque vectoring controller for electric vehicles. The proposed controller distributes drive/brake torque between the four wheels to achieve the desired handling response and, in addition, intervenes in the longitudinal dynamics in cases where the turning radius demand is infeasible at the speed at which the vehicle is traveling. The proposed controller is designed in the Nonlinear Model Predictive Control framework, which has recently shown great promise for real time implementation. Hence, the controller accounts for critical nonlinearities of the vehicle dynamics in limit handling conditions and constraints from the actuators and tyre-road interaction. We implement the controller in a realistic, high fidelity simulation environment to demonstrate its performance.**

I. INTRODUCTION

Electric vehicles (EV) nowadays, have gained a lot of popularity not only regarding their important role as sustainable transportation systems but also for their performance in traction and stability. Having the ability of different propulsion system configurations, such as independent motors for each wheel, electric vehicles allow us to implement more efficient safety algorithms [1], [2]. One of the most trending safety algorithms is Torque Vectoring (TV) which allows control of the distribution of the total traction/braking torque between the four wheels of the vehicle. Typically, Torque Vectoring systems aim at controlling the lateral dynamics of the vehicle by tracking yaw rate, and occasionally sideslip angle, reference signals. The throttle/brake-pedal inputs are interpreted as a torque demand signal which should be respected by the summation of the four wheel applied torques. A popular approach for the design of a torque vectoring system is a hierarchical scheme, where a high level direct yaw moment controller (e.g. PID or sliding mode) feeds into the low level arbitrator, which distributes the torque demand to the available actuators to achieve the desired yaw moment [3]. Recently, the emergence of Model Predictive Control and efficient numerical algorithms, has made it possible for such techniques to be used in vehicle chassis control applications, delivering optimal solutions and incorporation of critical constraints in the calculation of the control action. In [4] a linear MPC technique is deployed using recursive linearisation of the vehicle dynamics, to achieve the desired handling response (yaw rate) by distributing the torque demand in the four wheels of an electric vehicle. Important actuator limits are taken into consideration in the form of input constraints, and the controller is successfully deployed on a test vehicle.

In the past few years it has been recognised that active control of the vehicle's velocity is a very effective control strategy in the limits of lateral acceleration. Expert human (race) drivers have developed the so-called Trail-Braking technique for negotiating corners at high speeds [5]. Trail-braking essentially refers to the simultaneous braking and steering action, which regulates the speed of the vehicle to the feasible value to negotiate the corner, exploits the full acceleration envelope at all times and imposes an oversteering and more agile response of the vehicle due to weight transfer effects. The observation of the importance of longitudinal control interventions during cornering is made by van Zaten et al. [6] pointing out that when the turning radius continuously changes, Electronic Stability Controls (ESC) yaw moment correction is not sufficient and a controlled velocity reduction is necessary. This resulted in one of the ESC new functions, velocity regulation, achieved by superimposing individual braking of all four wheels on the standard ESC intervention [7]. In [8] a proportional feedback control is used to show that velocity regulation is more effective than brake actuated yaw control, progressively increasing path curvature. In [9] a combined yaw stabilization and velocity regulation is presented to mitigate terminal under-steer using rear axle electric torque vectoring. The vehicle model incorporates nonlinear tyre characteristics and coupling of the longitudinal and lateral tyre forces and linear MPC designs are presented using recursive linearisation of the vehicle dynamics. Recently, the control design from [9] has been extended to nonlinear MPC in [10] and compared with previous linear approaches, both in terms of control objective achievement and demanded computational resource. It is worth noting that the control scheme of both [9] and [10] does not take into consideration any torque demand by the driver. The controller aims at stabilizing the lateral dynamics of the vehicle and tracking a speed reference determined from the steering input of the driver in order for the requested turning radius to be feasible. In addition, this approach does not consider the modification of the handling behavior of the vehicle, as for instance in [3] where the understeer gradient of the controlled vehicle is actively modified by the torque vectoring system.

In this paper we present the development of a torque vectoring controller to distribute the requested drive/brake torque to the four wheels of an electric vehicle to control the longitudinal and lateral dynamics. In addition to the approaches of [3] and [4] the controller is designed to

K. Zarkadis, E. Velenis (corresponding author) and S. Longo are with the Advanced Vehicle Engineering Centre, School of Aerospace, Transport and Manufacturing, Cranfield University, College Road, Cran- field, Bedfordshire, MK43 0AL, U.K. (k.zarkadis, e.velenis, s.longo)@cranfield.ac.uk E. Siampis is with Delta Motorsport, Silverstone Technology Park, Towcester NN12 8GX, U.K. stathis@delta-motorsport.com

intervene to the longitudinal dynamics of the vehicle in cases of overspeeding in a cornering maneuver. The controller delivers an on-demand modified lateral dynamics response and aims to deliver the torque demand set by the driver in addition to the approach of [9] and [10]. We employ a nonlinear MPC (NMPC) design which accounts for vehicle dynamics nonlinearities and actuator limitations. In addition, the longitudinal intervention is integrated into the control design by introducing a feasible velocity constraint, rather than tracking a velocity reference as in [9] and [10]. The controller is implemented in a high fidelity simulation environment, IPG Carmaker, where its performance is demonstrated and the real time implementation capability is discussed.

II. VEHICLE AND TYRE MODEL

A. Vehicle Model

In this section we provide the vehicle dynamics model which is used to calculate the optimal control inputs by the Model Predictive Controller presented in the following section. As mentioned in the introduction, the controller is aimed to intervene in both longitudinal and lateral dynamics and hence longitudinal, lateral speed and yaw rate are the selected state variables of the model. Similar to common practice [10], [5], pitch, roll rotations and vertical vehicle body motion are neglected. The equations of motion (EoM) of the front wheel steering, four-wheel vehicle model (Fig.1) are

$$\begin{aligned} m\dot{V}_x = &(f_{FL_x} + f_{FR_x})\cos\delta - (f_{FL_y} + f_{FR_y})\sin\delta \\ &+ f_{RL_x} + f_{RR_x} + mrV_y, \end{aligned} \tag{1}$$

$$\begin{aligned} m\dot{V}_y = &(f_{FL_x} + f_{FR_x})\sin\delta + (f_{FL_y} + f_{FR_y})\cos\delta \\ &+ f_{RL_y} + f_{RR_y} - mrV_x, \end{aligned} \tag{2}$$

$$\begin{aligned} I_z\ddot{\psi} = &\, l_F[(f_{FL_x} + f_{FR_x})\sin\delta + (f_{FL_y} + f_{FR_y})\cos\delta] \\ &- l_R(f_{RL_y} + f_{RR_y}) \\ &+ w_L(-f_{FL_x}\cos\delta + f_{FL_y}\sin\delta - f_{RL_x}) \\ &+ w_R(f_{FR_x}\cos\delta - f_{FR_y}\sin\delta + f_{RR_x}), \end{aligned} \tag{3}$$

where m is the mass of the vehicle, V_x and V_y are the longitudinal and lateral vehicle velocity at its Center of Mass (CM) respectively, δ is the steering angle on both the front wheels, r is the yaw rate and I_z is the vehicle's moment of inertia about the vertical axis. Finally, l_F , l_R, w_L and w_R determine the location of the center of each wheel with respect to the CM. The longitudinal and lateral tyre forces are denoted by f_{ij_k} ($i = F, R$, $j = L, R$ and $k = x, y$), while the rolling resistances at the tyres have been neglected.

In the EoM above we consider the steering angle as a parameter provided by the driver. The longitudinal tyre forces are calculated from wheel torque rate control inputs and vertical wheel loads (SIII), whereas the lateral tyre forces are provided as functions of the corresponding tyre slip angle as described in the following.

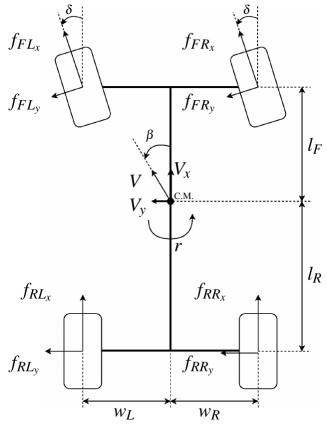

Fig. 1: Vehicle model

B. Tyre Model

By neglecting the pitch and roll rotation along with the vertical motion of the sprung mass of the vehicle, the vertical force f_{ij_z} on each wheel is calculated using the static load distribution and longitudinal and lateral weight transfers [11]

$$\begin{aligned} f_{FL_z} &= f^0_{FL_z} - \Delta f^x_L - \Delta f^y_F, \\ f_{FR_z} &= f^0_{FR_z} - \Delta f^x_R + \Delta f^y_F, \\ f_{RL_z} &= f^0_{RL_z} + \Delta f^x_L - \Delta f^y_R, \\ f_{RR_z} &= f^0_{RR_z} + \Delta f^x_R + \Delta f^y_R, \end{aligned}$$

$$\begin{aligned} \Delta f^y_F &= \frac{mhl_R}{(l_F + l_R)(w_L + w_R)} a_y, \\ \Delta f^y_R &= \frac{mhl_F}{(l_F + l_R)(w_L + w_R)} a_y, \\ \Delta f^x_L &= \frac{mhw_R}{(l_F + l_R)(w_L + w_R)} a_x, \\ \Delta f^x_R &= \frac{mhw_L}{(l_F + l_R)(w_L + w_R)} a_x, \end{aligned} \tag{4}$$

where $f^0_{ij_z}$ is the static vertical force distribution, Δf^y_F and Δf^y_R the weight transfer along the lateral body axis resulting from lateral acceleration a_y and Δf^x_L and Δf^x_R the weight transfer along the longitudinal body axis resulting from longitudinal acceleration a_x.

As mentioned before the longitudinal forces in EoM (1)-(3) are considered as the control inputs of the vehicle dynamics. Neglecting the dynamics of wheel rotation we can associate the normalised longitudinal tyre forces μ_{ij_x} with the applied wheel torques as follows:

$$\mu_{ij_x} = \frac{T_{ij}}{f_{ij_z} R_w}, \tag{5}$$

where T_{ij} is the torque of each wheel and R_w the wheel's radius.

Next we introduce a model for the calculation of the lateral tyre forces, which includes the dependence on tyre slip angle (cornering stiffness), a linear dependency on the normal force and the coupling with the longitudinal tyre forces.

Using the friction circle concept, the maximum lateral tyre force coefficient $\mu_{ij_y}^{\max}$ is given by the tyre-road friction coefficient mu and the controlled longitudinal tyre force coefficient μ_{ij_x}:

$$\mu_{ij_y}^{\max} = \sqrt{\mu^2 - \mu_{ij_x}^2}. \tag{6}$$

The lateral force coefficient is then calculated as a linear function of the tyre slip angle, saturated by the above $\mu_{ij_y}^{\max}$ limit.

$$\mu_{ij_y} = -sign(\alpha_{ij}) \cdot min(\mu_{ij_y}^{\max}, n_{ij}|\alpha_{ij}|), \tag{7}$$

where α_{ij} is the slip angle at each of the four tyres, and n_{ij} is the cornering stiffness coefficient of each tyre defined as the ratio of tyre cornering stiffness divided by the normal force at each tyre.

In order to avoid the non-smoothness at the point of saturation in equation (7), we propose to use an approximation of this expression using the Logistic function [12] as follows:

$$\mu_{ij_y} = \frac{2\mu_{ij_y}^{\max}}{1 + e^{k(n_i\alpha_{ij})}} - \mu_{ij_y}^{\max}. \tag{8}$$

In the above equation k is the steepness of the curve and is tuned according to the cornering stiffness coefficient of the tyre. As we can see in Fig.2 the saturating equation (8) not only follows the boundaries but is smoother than the one corresponding to (7). Finally, the longitudinal and lateral tyre forces are calculated using the normal force at each tyre as follows:

$$f_{ij_x} = f_{ij_z}\mu_{ij_x} \quad \text{and} \quad f_{ij_y} = f_{ij_z}\mu_{ij_y} \tag{9}$$

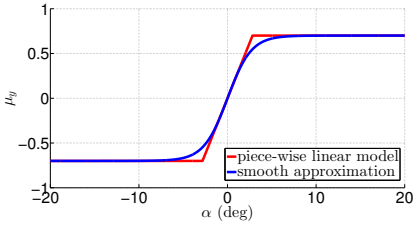

Fig. 2: Lateral road coefficient approximation

III. NONLINEAR MPC FORMULATION

The MPC design is cast in the sampled-data framework by discretising the continuous-time plant and the associated quadratic cost function. For the nonlinear continuous-time system $\dot{x} = f_c(x, u)$ with state and input x and u respectively, the discrete optimal control is

$$\begin{aligned} \min_{x,u} & \sum_{k=0}^{N-1} (x_k - x_{ref})^T Q_n (x_k - x_{ref}) \\ & + (u_k - u_{ref})^T R_n (u_k - u_{ref}) \\ s.t. \quad & x_0 = x_{in} \\ & x_{k+1} = f_d(x_k, u_k), \quad k = 0, ..., N-1 \\ & x_k^{min} \leqslant x_k \leqslant x_k^{max}, \quad k = 0, ..., N-1 \\ & u_k^{min} \leqslant u_k \leqslant u_k^{max}, \quad k = 0, ..., N-1 \end{aligned} \tag{10}$$

where N is the prediction horizon and Q_n, R_n are the weighting matrices [13].

A. Cost Function

Based on the above standard MPC theory, a dense MPC problem using soft constraining on the state [14] is formulated for application in this paper. In addition we choose as state vector for the controller to be $X = [V_x \quad V_y \quad r \quad T_{ij}]$ and as control input the rate of torque for each wheel $U = [\Delta T_{ij}]$. As disretisation method for the continuous internal model of the MPC we used the Runge-Kutta 4^{th} order (RK4). The additional equation for wheel torque dynamics is:

$$T_{ij_{k+1}} = T_{ij_k} + \Delta T_{ij_k} \tag{11}$$

The main objective of the controller is to track a yaw rate reference and respect the driver's torque demand while at the same time regulating the velocity so that it stays within a feasible region. Therefore, the objective function is defined as

$$\begin{aligned} J = \sum_{k=0}^{N-1} & q_r(r - r_{ref})^2 + q_T(T_{dmd} - T_{veh})^2 + q_u U^2 \\ & + \rho_r e_r + \rho_V e_V \end{aligned} \tag{12}$$

The first term in the cost function relates to the yaw rate tracking error. As common practice suggests [3], we use a linear steady-state bicycle model with the desired handling characteristic (understeer gradient) to create the reference yaw rate:

$$r_{ref} = \delta \frac{V_x}{L + K_{und} V_x^2}, \tag{13}$$

where L is the length of the vehicle and K_{und} is the desired understeer gradient. We assume the reference to be constant and equal to the current value over the prediction horizon. The second term in (12) is defined such that the controller meets the drivers torque demand, where T_{veh} is the summation of all four wheel torques T_{ij}. The third term introduces penalisation of the control inputs where q_r, q_T and q_u in front of each term are their corresponding weights. The last two terms are used to soften the yaw rate and velocity constraint respectively. All the weight values used are shown in TABLE I where ϵ defines a small threshold around V_{lim} ($\epsilon = 1m/s$).

TABLE I: Weighting parameters.

Weight	$V < V_{lim} - \epsilon$	$V_{lim} - \epsilon \leqslant V \leqslant V_{lim}$	$V > V_{lim}$
q_r	1	0.1	1
q_T	$\frac{1}{(4 \cdot T_{max})^2}$	$\frac{0.01}{(4 \cdot T_{max})^2}$	$\frac{1}{(4 \cdot T_{max})^2}$
q_u	$\frac{1}{(\Delta T_{safe} \cdot T_s)^2}$	$\frac{0.1}{(\Delta T_{safe} \cdot T_s)^2}$	$\frac{1}{(\Delta T_{safe} \cdot T_s)^2}$
p_r	1000	1000	1
p_V	1000	1000	1

B. State Constraints

As discussed in the introduction, the aim of the proposed controller is to intervene in the longitudinal dynamics, when the requested lateral acceleration is infeasible for the given velocity of the vehicle.

From the steady-state equations of the bicycle model the reference yaw rate corresponds to a reference lateral acceleration, which is limited by the available tyre-road friction coefficient (grip)

$$a_{y_{ref}} = V r_{ref} \leqslant \mu g, \tag{14}$$

where g is the acceleration of gravity and V is the current vehicles total speed [15]. The above can be interpreted as a limit is vehicle speed such that the requested yaw rate (or lateral acceleration) is feasible:

$$V_{lim} = g\frac{\mu}{r_{ref}}. \tag{15}$$

This translates to a state constraint:

$$\left|\frac{V_x}{cos\beta}\right| \leqslant V_{lim} + e_V, \tag{16}$$

which is implemented as a soft constraint with slack variable $e_V \geqslant 0$. It is important to note that we implement a soft constraint at this stage because the yaw rate reference is generated by the driver's steering input and there are no guarantees that the constraint will be respected. The control action to reduce the speed (brake) in order to satisfy the constraint (16) is herein referred to as Active Trail-Braking.

Similar to [9], [10] we impose a yaw rate constraint to increase the robustness of the controller and soften it as:

$$|r| \leqslant r_{lim} + e_r, \tag{17}$$

where $e_r \geqslant 0$ is the corresponding slack variable and r_{lim} is calculated using the current total vehicle velocity V:

$$r_{lim} = g\frac{\mu}{V}. \tag{18}$$

Finally we also constraint the torques of each wheel

$$T_{ij}^{min} \leqslant T_{ij} \leqslant T_{ij}^{max}, \tag{19}$$

where T_{ij}^{min} and T_{ij}^{max} are given from the motor torque graph.

C. Input Constraints

Constraints are also set on the control inputs ΔT_{ij} so that the rates of torque on the wheels never exceed the maximum allowable torque change for both motor and battery safe operations

$$|\Delta T_{ij}| \leqslant \Delta T_{safe} T_s, \tag{20}$$

where ΔT_{safe} is given by the electric motor supplier. All the parameters used for the vehicle and tyre model can be seen in TABLE II.

TABLE II: Vehicle properties.

Parameter (Unit)	Description	Value
m (kg)	mass	1137
L (m)	wheelbase	2.5
R_w (m)	wheel radius	0.298
h (m)	height of C.M.	0.317
I_z (kg·m^2)	yaw inertia of vehicle	1174
l_F (m)	front axle to C.M. distance	1.187
l_R (m)	rear axle to C.M. distance	1.313
w_L (m)	left wheels to C.M. distance	0.687
w_R (m)	right wheels to C.M. distance	0.687
ΔT_{safe} (Nm/s)	motor/battery torque rate limit	10000
T_{max} (Nm)	motor's maximum torque	700
T_{min} (Nm)	motor's minimum torque	-500

IV. SIMULATION RESULTS

In the following section we compare the MPC strategy against an uncontrolled vehicle without torque vectoring using the high fidelity vehicle model and the driver model available in CarMaker (CM). The vehicle model in CM is naturally understeer and we simulate in a road coefficient $\mu = 0.7$. The NMPC strategy employs the Primal Dual Interior Point (PDIP) method as available in FORCES Pro [16] where we configured a sampling time and horizon for the controller of $T_s = 0.03s$ and $N = 10$ steps respectively, and a total number of 300 solving iterations. For the reference generation vehicle model we assume an oversteer gradient coefficient $K_{und} = -1\,\mathrm{deg}/s$. The simulation studies are made on a laptop computer (i7-4710HQ at 2.50 GHz with 16 GB of RAM memory).

A. Step-steer scenario

In this scenario we examine the controller's response in a step steer maneuver. We assume a constant torque demand by the driver $T_{dmd} = 1000Nm$ with initial velocity $V_{in} = 30km/h$ and apply a steering wheel input $\delta = 90\,\mathrm{deg}$ after 2 seconds.

In Fig.3a the importance of the velocity constraint is easily observed. The uncontrolled vehicle exceeds the required velocity needed in order to take the turn whereas the constrained NMPC reaches the steady state velocity quickly. The Trail-braking intervention occurs without inducing excessive values of sideslip angle as presented in Fig.3b. Violating the constraint does not result to instability or incontrollable state. A similar conclusion can be made about the yaw rate in Fig.3c where the uncontrolled vehicle has a totally different response than the reference steady state model but the controlled version respects both the soft constraint and reference.

In Fig.3d we can see the controlled torques fed to the wheels of the vehicle. When the steering input is given, the vehicle starts braking in order to meet the velocity constraint and then goes to a steady state response keeping the outer wheel torques higher than the inner ones. It is also important to note that the total torque of the wheels never exceeds the driver's torque demand. The computational performance shown in Fig.3e proves that since the solve time of the controller to find an optimal solution under the specified

horizon is less than its sampling time, the controller runs in real-time on this hardware reaching a maximum number of 226 iterations. Finally, in Fig.4 we demonstrate a top view of the step steer maneuver under different understeer gradients using the NMPC. The blue path corresponds to the results shown above with a ($K_{und} = -1\,\mathrm{deg}/s$) whereas the pink and red ones are the neutralsteer ($K_{und} = 0\,\mathrm{deg}/s$) and oversteer ($K_{und} = +1\,\mathrm{deg}/s$) targets respectively.

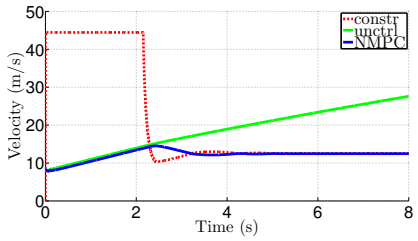

(a)

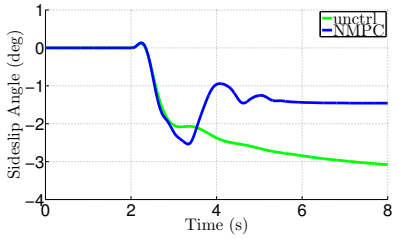

(b)

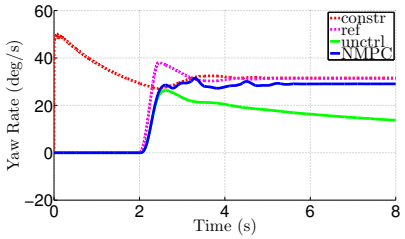

(c)

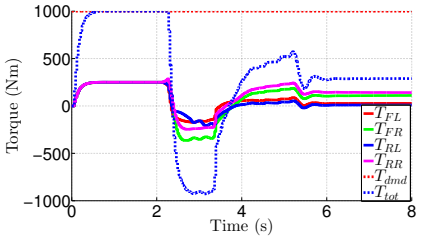

(d)

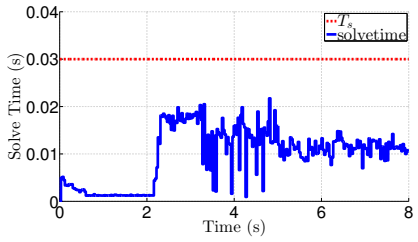

(e)

Fig. 3: Step Steer maneuver: (a) vehicle velocity; (b) sideslip angle; (c) yaw rate; (d) individual wheel torques & total torque; (e) NMPC computational time

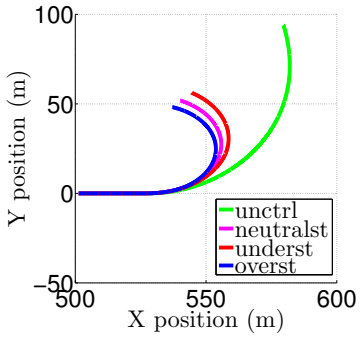

Fig. 4: Step Steer maneuver trajectory

B. *Double lane change scenario*

In the double lane change maneuver we assume a torque demand $T_{dmd} = 1000Nm$ and initial velocity $V_{in} = 5km/h$. As we notice from both Fig.5a and Fig.5c the controlled vehicle effectively completes the double lane change scenario even though the velocity mostly exceeds the constraint whereas the uncontrolled vehicle becomes unstable on the final lane change. The resulting instability of the uncontrolled vehicle is also evident in the increase of sideslip angle (Fig5b), whereas the controlled vehicle completes the maneuver maintaining low values of sideslip.

The wheel torques shown in Fig.5d meet the criteria of the torque vectoring control method where the outer wheels have greater torques than the inner wheels when the vehicle is turning and then finally converge to the same value at the end of the maneuver, with a small torque variation between the rear and front wheels affected by the weighting factors. However, as we can see from Fig.5b and Fig.6, the driver regains control of the vehicle thanks to the collaboration of both the velocity regulation and TV. The Trail-Braking interventions, in cases of active velocity constraints, are also evident in the total applied torque. Finally, the presented computational times of the NMPC in Fig.5e prove once again that it runs in real-time on the current hardware system reaching a maximum number of 203 iterations.

V. CONCLUSIONS

In this paper we presented the development of a torque vectoring control system which distributes the requested torque demand between the four wheels of the vehicle to achieve the desired handling response. The novel feature of the controller is the provision of longitudinal acceleration interventions in order to regulate the vehicle speed in a region where the requested lateral acceleration becomes feasible. This combined braking and cornering action of the controller is similar to techniques employed by expert human drivers and referred herein as Active Trail-Braking.

The controller was designed in a nonlinear model predictive control framework which allows for critical nonlinearities of the vehicle dynamics model, as well as constraints

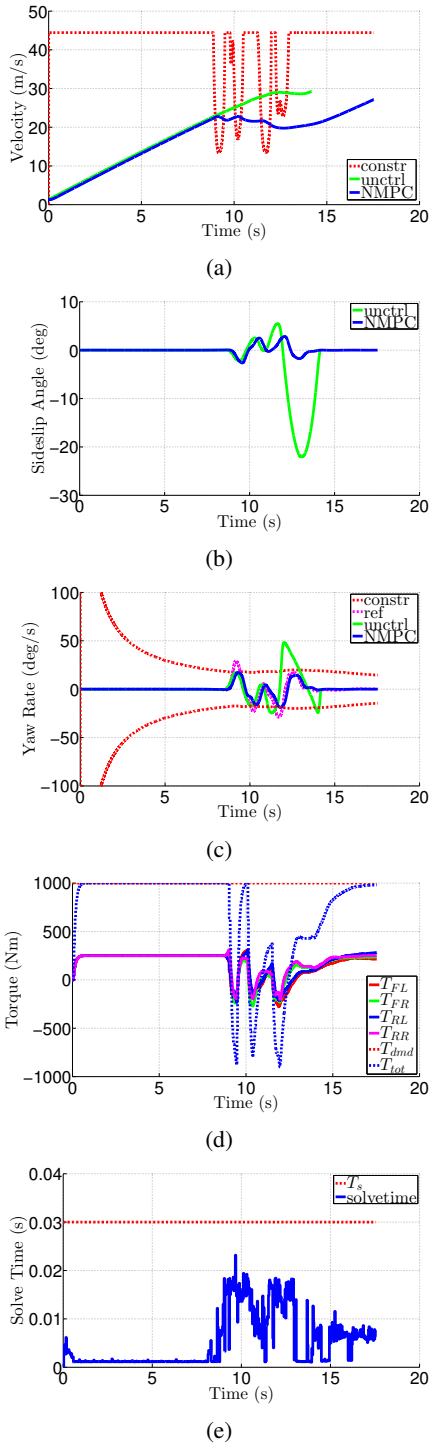

Fig. 5: Double Lane Change maneuver: (a) vehicle velocity; (b) sideslip angle; (c) yaw rate; (d) individual wheel torques & total torque; (e) NMPC computational time

associated with actuator limitations to be accounted for. The controller was implemented in a high fidelity simulation environment to demonstrate its performance. The required computational time is recorded and we conclude that current numerical nonlinear optimal control solvers are capable of being deployed in real time for such demanding applications, in a receding horizon implementation, with the chosen sampling time and optimization horizon length.

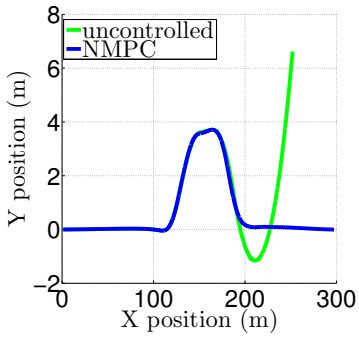

Fig. 6: Double Lane Change maneuver trajectory

References

[1] Smith, E. N., Velenis, E., Tavernini, D., & Cao, D. (2017). Effect of handling characteristics on minimum time cornering with torque vectoring. Vehicle System Dynamics, 1-28.

[2] Basrah, M. S., Siampis, E., Velenis, E., Cao, D., & Longo, S. (2017). Wheel slip control with torque blending using linear and nonlinear model predictive control. Vehicle System Dynamics, 1-21.

[3] De Novellis, L., Sorniotti, A., Gruber, P., Orus, J., Fortun, J. M. R., Theunissen, J., & De Smet, J. (2015). Direct yaw moment control actuated through electric drivetrains and friction brakes: Theoretical design and experimental assessment. Mechatronics, 26, 1-15.

[4] Jalali, M., Khajepour, A., Chen, S. K., & Litkouhi, B. (2016). Integrated stability and traction control for electric vehicles using model predictive control. Control Engineering Practice, 54, 256-266.

[5] Velenis, E., Tsiotras, P., & Lu, J. (2008). Optimality properties and driver input parameterization for trail-braking cornering. European Journal of Control, 14(4), 308-320.

[6] Van Zanten, A. T. (2000). Bosch ESP systems: 5 years of experience (No. 2000-01-1633). SAE Technical Paper.

[7] Liebemann, E. K., & Fuehrer, D. I. T. (2007). More safety with vehicle stability control (No. 2007-01-2759). SAE Technical Paper.

[8] Gordon, T., Klomp, M., & Lidberg, M. (2012). Control mitigation for over-speeding in curves: Strategies to minimize off-tracking. In Proceedings of the 11th International Symposium on Advanced Vehicle Control (AVEC'12).

[9] Siampis, E., Velenis, E., & Longo, S. (2015). Rear wheel torque vectoring model predictive control with velocity regulation for electric vehicles. Vehicle System Dynamics, 53(11), 1555-1579.

[10] Siampis, E., Velenis, E., Gariuolo, S., & Longo, S. (2017). A Real-Time Nonlinear Model Predictive Control Strategy for Stabilization of an Electric Vehicle at the Limits of Handling. IEEE Transactions on Control Systems Technology.

[11] Velenis, E., Katzourakis, D., Frazzoli, E., Tsiotras, P., & Happee, R. (2011). Steady-state drifting stabilization of RWD vehicles. Control Engineering Practice, 19(11), 1363-1376.

[12] Kyurkchiev, N., & Markov, S. (2015). Sigmoid functions: some approximation and modelling aspects. Some Moduli in Programming Environment Mathematica,(LAP Lambert Acad. Publ., Saarbrucken, 2015) ISBN, 978-3.

[13] Astrom, K. J., & Wittenmark, B. (1997). Computer-controlled systems: theory and design. Prentice-Hall.

[14] Maciejowski, J. M. (2002). Predictive control: with constraints. Pearson education.

[15] Rajamani, R. (2012). Lateral vehicle dynamics. In Vehicle Dynamics and Control (pp. 15-46). Springer US.

[16] Domahidi, A., & Jerez, J. (2014). FORCES Professional. embotech GmbH (http://embotech. com/FORCES-Pro). J uly.